Itinerant Helimagnetic Single-Crystalline MnSi Nanowires

Kwanyong Seo,[†,¶] Hana Yoon,[†,¶] Seong-Wan Ryu,[‡] Sunghun Lee,[†] Younghun Jo,[§] Myung-Hwa Jung,[⊥] Jinhee Kim,[∥] Yang-Kyu Choi,[‡] and Bongsoo Kim[†,*]

[†]Department of Chemistry, KAIST, Daejeon 305-701, Korea, [‡]Department of Electrical Engineering and Computer Science, KAIST, Daejeon 305-701, Korea, [§]Quantum Material Research Team, KBSI, Daejeon 305-333, Korea, [⊥]Department of Physics, Sogang University, Seoul 121-742, Korea, and [∥]Center for Nanoscience and Quantum Metrology, KRISS, Daejeon 305-600, Korea. [¶]These authors contributed equally to this work.

ABSTRACT We report the synthesis of free-standing MnSi nanowires *via* a vapor transport method with no catalyst and measurements of their electrical and magnetic properties for the first time. The single-crystalline MnSi nanowire ensemble with a simple cubic (B20) crystal structure shows itinerant helimagnetic properties with a T_c of about 30 K. A single MnSi nanowire device was fabricated by a new method using photolithography and a nanomanipulator that produces good ohmic contacts. The single-nanowire device measurements provide large (20%) negative magnetoresistance and very low electrical resistivity of 544 $\mu\Omega$cm for the MnSi nanowire.

KEYWORDS: nanowires · transition metal silicides · MnSi · single crystalline · nanodevices · magnetic materials

Research on the electromagnetic properties of metallic MnSi has attracted great attention in recent years with regard to the non-Fermi liquid behavior as well as its interesting applications. Behavior of electrons in metal is one of the key topics in condensed matter physics, and most of them can be explained well by the Landau−Fermi liquid theory.[1] Anomalous electron behavior has been, however, observed in some materials including high-temperature superconductor,[2] and the origin of this non-Fermi liquid behavior remains controversial.

MnSi has a B20-type simple cubic crystal structure without space inversion symmetry, leading to itinerant helimagnetic order below low temperature of about 30 K by Dzyaloshinski−Moriya (DM) spin−orbit interaction.[3] In particular, the electrical resistivity of MnSi shows anomalous temperature dependence above certain pressure (P_c = 14.6 kbar), which has been widely investigated for clear understanding of non-Fermi liquid behavior.[4−8] Temperature dependence of heat capacity of MnSi has been recently reported,[9] suggesting that MnSi is one of the novel and economic magnetocaloric materials showing temperature change under applied magnetic field. Other types of Mn−Si alloys also have been attracting much interest because of their complex structural diversities and intriguing physical properties. A group of semiconducting $MnSi_{2-x}$ distinguished as higher manganese silicides (HMS) is regarded as promising candidates for possible applications in spintronics, thermoelectrics, and silicon-based optoelectronics.[10−13]

It is important to synthesize MnSi in one-dimensional nanowire (NW) form because of the following reasons. First, making a perfectly single-crystalline NW without defects, dislocations, or grain boundaries is easier than the perfect bulk crystal form. Such perfectly single-crystalline NWs are indispensable for clear understanding of various physical phenomena as well as for applications. Perfectly single-crystalline MnSi NWs, particularly, may provide a hint to elucidate the non-Fermi liquid behavior that has not been clearly understood so far by the study of their physical properties. Second, in the application fields of spintronics, photovoltaics, and thermoelectrics, fabrications of the nanodevices with improved efficiency would become possible by employing NWs.[14−17] Third, NWs often reveal interesting physical properties different from those of their bulk counterpart. For example, CoSi NW shows ferromagnetic properties in contrast to the diamagnetic CoSi in bulk.[18]

Recently, synthesis of HMS NWs has been reported. Higgins *et al.* synthesized $Mn_{19}Si_{33}$ NWs by a MOCVD method and reported it as a first example of Nowotny chimney ladder (NCL) phase NW.[19] Ham *et al.* also synthesized semiconducting Mn_4Si_7 NWs that are ferromagnetic with higher T_c of 120 K than the bulk form (T_c = 40 K).[20]

Herein we report the synthesis of free-standing single-crystalline MnSi NWs by a

*Address correspondence to bongsoo@kaist.ac.kr.

Received for review November 18, 2009 and accepted April 23, 2010.

Published online April 28, 2010. 10.1021/nn901653q

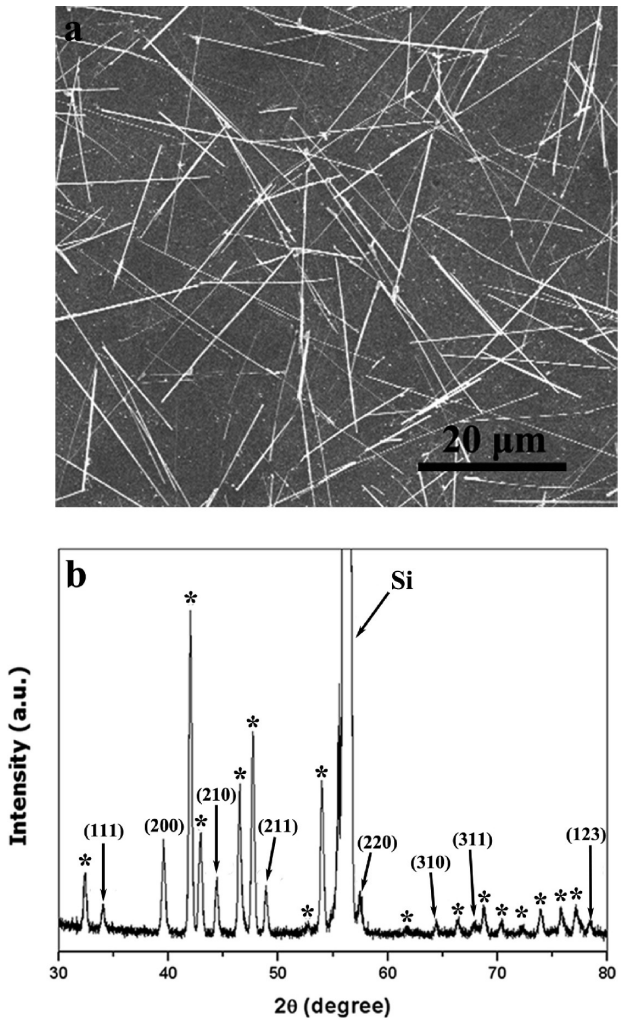

Figure 1. (a) Representative SEM image of MnSi NWs. (b) XRD pattern of the MnSi NWs on silicon substrate. The asterisks in panel b indicate the peaks from $MnSi_{1.7}$ film.

vapor transport method and measurements of electrical and magnetic properties of the NW for nanoscale device applications. The MnSi NWs show itinerant helimagnetic order with T_c of about 30 K and metallic properties with very low electrical resistivity of 544 μΩcm. A single MnSi NW device for the measurements was fabricated by a novel method employing photolithography and nanomanipulator to produce good ohmic contact between the NW and electrode. Measured magnetoresistance (MR) shows a large value of about 20% around T_c. Single-crystalline MnSi NWs may provide opportunities to investigate complex physical phenomena in detail and to develop high-efficient NW-based devices such as nanospintronics or a nanoscale magnetic refrigerator.

RESULTS AND DISCUSSION

Morphology, Structure, and Growth Mechanism. Representative field emission scanning electron microscopy (FESEM) image in Figure 1a shows MnSi NWs with straight morphology and lengths of tens of micrometers. The SEM and transmission electron microscopy (TEM) images (Figure 2) clearly show the NWs with a clean and smooth surface and a diameter of 70−150 nm. X-ray diffraction (XRD) spectrum in Figure 1b shows a typical pattern of the MnSi NWs. Observed peaks in the spectrum were successfully indexed to the cubic B20-type MnSi with a lattice constant 4.556 Å (space group $P2_13$, JCPDS card no. 81-0485). Interestingly, we observed peaks from $MnSi_{1.7}$, as denoted with asterisks in Figure 1b. The $MnSi_{1.7}$ peaks, one of the HMS, could have been from the $MnSi_{1.7}$ film formed on the Si substrate before the growth of MnSi NWs. XRD measurement for the sample in which only the film was synthesized without NWs showed only the $MnSi_{1.7}$ peaks. We provide cross-sectional SEM images of the NW/thin film interface in Figure S1 (Supporting Information). Such film growth has been observed often in the synthesis of silicide NWs, where the NWs could grow on the thin film through the diffusion of precursor atoms.[21,22] In the beginning stage of precursor evaporation, the degree of supersaturation of Mn precursor can be high, and thus the Mn precursor produces a silicide film on a Si substrate prior to the MnSi NWs growth. When the degree of supersaturation gets lower as the precursor evaporation proceeds, the MnSi NWs can grow on the silicide film.[23,24] Because the Si substrate under the film supplied Si atoms continuously to the film, the film would have Si-rich elemental composition of $MnSi_{1.7}$. A large unit cell of the tetragonal $MnSi_{1.7}$ tends to prevent formation of ultrathin film on a Si substrate,[25] as we observed thick film on the Si substrate in this experiment (Figure 3c).

To characterize the chemical composition and crystal structure of a single MnSi NW, we carried out energy-dispersive X-ray spectrometry (EDS), high-resolution TEM (HRTEM), and selected-area electron diffraction (SAED) studies. Figure 2a shows the TEM image and SAED pattern obtained from a representative MnSi NW. The diffraction pattern of the NW shows a regular spot pattern, confirming the single-crystalline nature of the NWs. The spots can be fully indexed to the cubic B20-type MnSi and demonstrate that the NW growth is along the [110] direction down the $[\bar{1}11]$ zone axis. Figure 2b shows a HRTEM image of a 70 nm diameter NW with clear lattice fringes, confirming again the single-crystallinity. The lattice spacing of the plane was measured to be 0.32 nm, agreeing well with the spacing of the (110) plane of a cubic MnSi structure. The two-dimensional fast Fourier transform (FFT) of the lattice resolved image obtained from the HRTEM (inset in Figure 2b) can also be indexed to a cubic B20 MnSi structure. Figure 2c shows a TEM-EDS spectrum of an individual MnSi NW. The analysis of a TEM-EDS spectrum confirms that the NW contains only Mn and Si in about 1:1 atomic ratio (the peak for Cu is from the grid). Moreover, detailed EDS study from the tip and the stem of a single NW does not show significant deviation from the 1:1 atomic ratio. HRTEM image confirmed that the

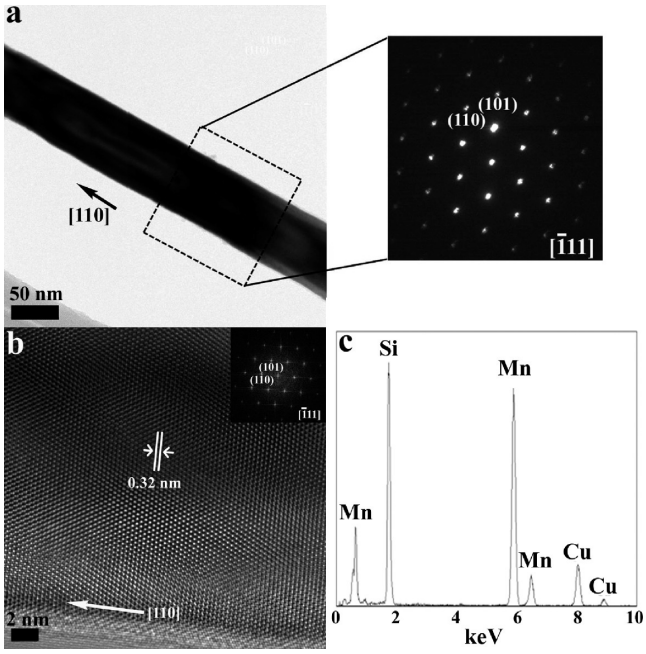

Figure 2. (a) TEM image and SAED pattern of MnSi NW. The SAED pattern is indexed for a simple cubic MnSi NW down the [$\bar{1}$11] zone axis. (b) HRTEM image. The labeled distance of 0.32 nm corresponds to the (110) plane, and the arrow shows the [110] growth direction. Inset in panel b shows two-dimensional fast Fourier transform (FFT) from the HRTEM. (c) TEM-EDS spectrum of an individual MnSi NW.

MnSi NWs are surrounded by an amorphous silica layer less than 4 nm thick (Supporting Information, Figure S2).

Recently, metal halide precursors have been used extensively for the synthesis of various metal silicide NWs. For example, $CoCl_2$ and FeI_2 precursors directly react with Si substrate at high temperature to form CoSi and FeSi NWs, respectively.[18,26,27] In this work, MnSi NWs were synthesized by the direct reaction of $MnCl_2$ vapor with a Si substrate that plays a dual role as a source of Si and a substrate where the Mn precursor vapor condensates to form silicide NWs. For the possible MnSi NW growth mechanism, vapor−liquid−solid (VLS) growth is unlikely because no catalyst metal particles or thin films are employed in the synthesis. In addition, the SEM and TEM images in Figures 1 and 2, respectively, do not show the presence of any metal catalyst on the NW tip. Hence, we suggest that the MnSi NWs are grown by a vapor−solid (VS) growth mechanism. Although VS growth mechanism has not been fully understood yet, it has been generally accepted that the concentration of precursor vapor plays an important role during the nucleation and growth of silicide nanostructures.[28−36] We also find that the vapor pressure of the Mn precursor is a very critical factor in the MnSi NWs growth. When either the temperature of the precursor heating zone or carrier gas flow rate was increased, leading to the higher vapor pressure of the Mn precursor, MnSi microstructures were produced instead of MnSi NWs (Figure 3a). The XRD data in Figure 3b and a cross-sectional view of the MnSi microstructure/$MnSi_{1.7}$ thin film inter-

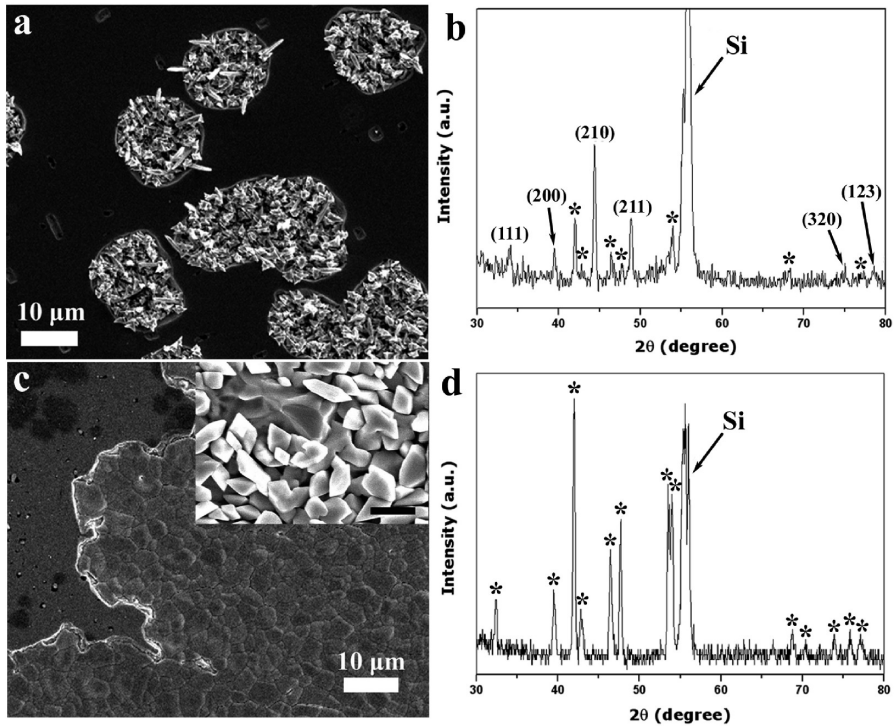

Figure 3. (a) SEM image of MnSi microstructures. (b) XRD pattern of the MnSi microstructures in panel a. (c) SEM image of the $MnSi_{1.7}$ film. Inset shows the magnified SEM image of the $MnSi_{1.7}$ microstructures. Scale bar is 2 μm. (d) XRD pattern of the $MnSi_{1.7}$ film and microstructures in panel c. Asterisks in panels b and d indicate peaks from $MnSi_{1.7}$.

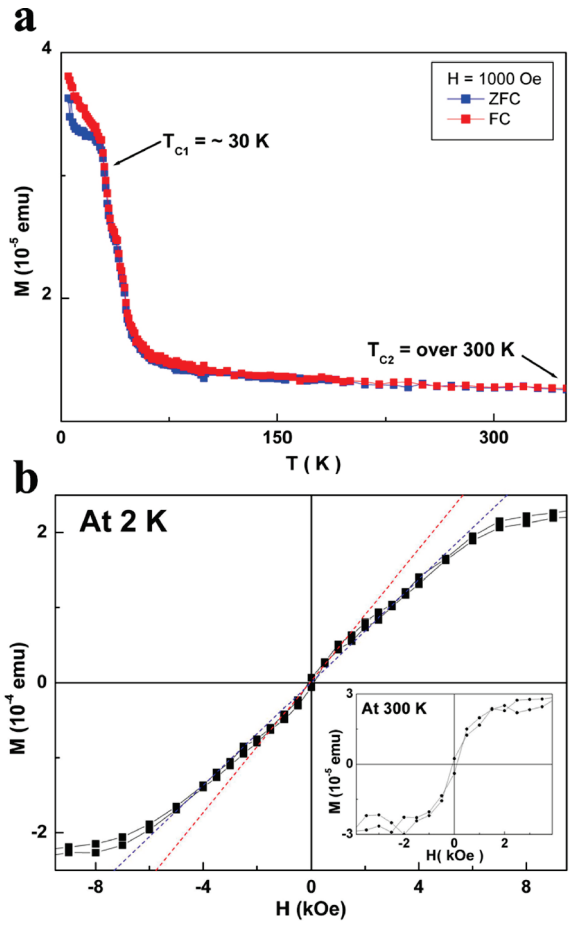

Figure 4. (a) Plot of *M vs T* obtained from MnSi NW ensemble at applied field of 1000 Oe. Red squares and blue squares represent the FC and ZFC data, respectively. (b) Plot of *M* as function of *H* obtained from the MnSi NW ensemble at 2 K. Red and blue dashed lines are a guide to the eye, which reflect two different magnetic behaviors. The inset shows a plot measured at 300 K.

face show that MnSi microstructures were grown on the $MnSi_{1.7}$ film, as were MnSi NWs (see Figure S1 in Supporting Information). In addition, only the film structure could be observed when the temperature of the substrate was increased by 100 °C, and microstructures were grown at lower pressure of 100−500 Torr (Figure 3c). We found that both the film and microstructures were a tetragonal $MnSi_{1.7}$. This could be caused by subtle increase in the degree of supersaturation as a consequence of change in temperature or pressure. Our experimental results are in accordance with previous reports in which high degree of supersaturation induces the growth of bulk crystals or film.[37−40]

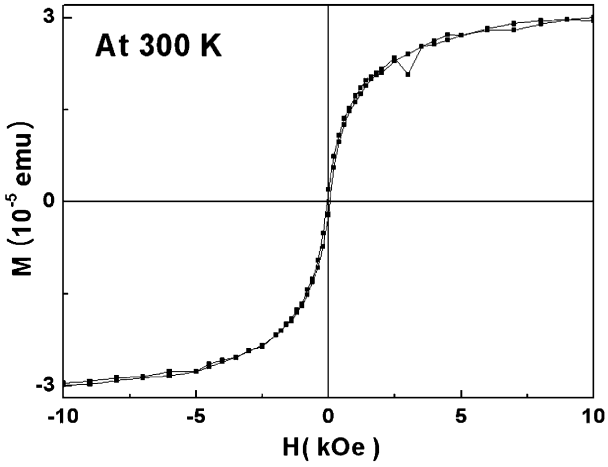

Figure 5. Plot of *M* as function of *H* obtained from the $MnSi_{1.7}$ film at 300 K.

Magnetic Properties. Detailed magnetic properties of the as-grown MnSi NW ensemble on a Si substrate have been studied by using a superconducting quantum interference device (SQUID) magnetometer. Figure 4a displays the temperature-dependent magnetization $M(T)$ curves measured under an applied field of 1000 Oe after zero-field cooling (ZFC) and field cooling (FC). Note that the $M(T)$ curves display two different magnetic behaviors showing T_c of about 30 K (T_{c1}) and of over 300 K (T_{c2}), respectively. The T_{c1} of about 30 K is consistent with the T_c of bulk MnSi with a B20 simple cubic crystal structure. The transport measurement on the single MnSi NW device verified that T_{c1} originates from a MnSi NW (Figure 7). However, the T_{c2} observed to be above 300 K is interesting because such high T_c has not been observed in any Mn−Si alloy yet. The magnetization as a function of magnetic field (Figure 4b) also shows a similar result to that of the $M(T)$ curve. The $M(H)$ curve at 2 K indicates two different ferromagnetic behaviors represented by red and blue dashed lines, respectively. At 2 K, both ferromagnetic components affect overall magnetic properties because the temperature is lower than T_{c1} of about 30 K. However, at 300 K, which is higher than T_{c1}, only one ferromagnetic behavior was observed because the material with T_{c1} of 30 K (MnSi NW) becomes paramagnetic at 300 K, as shown in the inset of Figure 4b. To verify that ferromagnetism at room temperature is induced by the $MnSi_{1.7}$ film and not by MnSi NWs, we obtained the $M(H)$ curve shown in Figure 5 only from the film after removing all MnSi NWs by a sonication process. This $M(H)$ curve is almost identical to the result for the MnSi NW ensemble grown on the film at 300 K (inset of Figure 4b). For CoSi NWs, strong ferromagnetic properties were induced when diameters are less than 30 nm due to high percentage of surface Co atoms.[18] However, the surface effect on the ferromagnetism of MnSi NWs would be quite low because their diameters are ~100 nm. We obtained the $M(H)$ curve at 40 K to check possible contribution from ferromagnetic Mn oxides, such as MnO (T_c of ~50 K) and Mn_3O_4 (T_c of ~40 K).[41,42] Most of other Mn oxides and metallic Mn are antiferromagnetic.[20] The $M(H)$ curve at 40 K showed a single ferromagnetic behavior (Supporting Information, Figure S3), as was observed at 300 K. Contribution from ferromagnetic Mn oxides to the observed magnetic properties of a MnSi NW ensemble thus can be excluded.

Device Fabrication and Transport Properties. Transport studies and MR measurements have been carried out

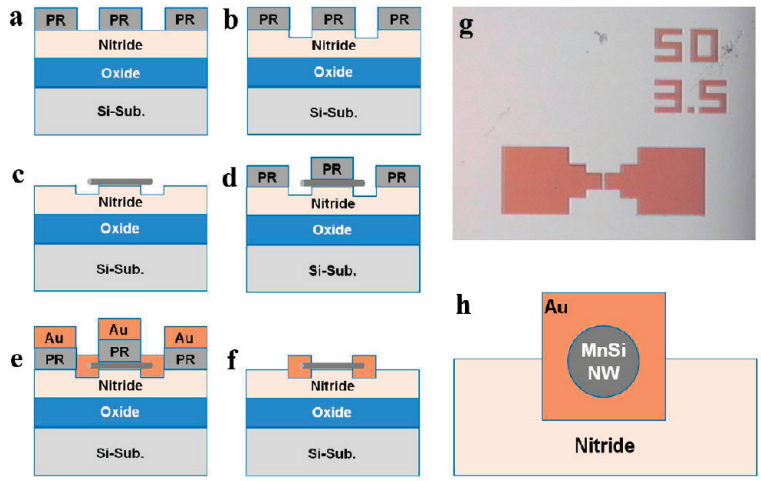

Figure 6. Schematic illustrations (cross-section view) for the fabrication process of a single MnSi NW device. To block Au diffusion and isolate the NW from the substrate, nitride and oxide layers were initially deposited on the silicon substrate followed by photoresist patterning as shown in panel a. The nitride layer was etched for the NW alignment and to allow three-dimensional ohmic contact between the NW and an electrode (panel b). After removing the photoresist (panel g, optical microscope image), a MnSi NW was positioned by a nanomanipulator between two pad areas (panel c). The photoresist was patterned again, and Au was evaporated on top of the wafer (panels d and e). Finally, the photoresist was lifted off in an acetone solvent (panel f). The NW is wrapped three-dimensionally by a Au electrode (panel h).

on a single MnSi NW. The device for the measurements was prepared by a novel method using a photolithography technique and a nanomanipulator following the process shown in Figure 6. Although we tried several times to fabricate the device using a standard e-beam lithography technique, it was difficult to form ohmic contacts between the NW and electrodes due to an amorphous silica layer covering the MnSi NW. For our new method applied in this work, however, NW is three-dimensionally wrapped with an electrode material whereas the electrode is two-dimensionally covered in the standard e-beam lithography technique, thus this new method facilitates the formation of ohmic contact after further treatment resulting from an increased contact area between the NW and electrode (Figure 6h).

Figure 7b shows a linear behavior of current−voltage ($I-V$) curve for a single MnSi NW device fabricated by this new method. The resistivity measured at room temperature is found to be 544 μΩcm. The higher resistivity than a bulk value (220 μΩcm)[43] is ascribed to the contact resistance between the NW and electrodes due to the two-probe configuration. Figure 7c shows the temperature-dependent resistance measured under external magnetic fields. A peak of dR/dT around 30 K is induced by the carrier scattering from spin fluctuations near T_c and agrees well with the result for bulk MnSi.[3] Furthermore, we observed a resistance change under external magnetic fields, ascribed to suppression of the scattering by the external magnetic field. The temperature-dependent MR, defined as $MR = [R(9T) - R(0T)]/R(0T)$, was measured under external magnetic fields and shows a large negative value of −20% near T_c at an applied field of 9 T (Figure 7d). The observed temperature dependence of the magnetic properties of a MnSi NW indicates that the NW has the same itinerant ferromagnetic properties as bulk MnSi[3] and confirms again that T_{c1} of about 30 K observed in the SQUID measurement originates from MnSi NWs. The newly synthesized single-crystalline MnSi NWs would provide opportunities for fundamental research as well as for NW-based applications such as magnetocaloric effect.

CONCLUSION

We synthesized single-crystalline free-standing MnSi NWs by the vapor transport method for the first time. Magnetic measurements of the MnSi NW ensemble show two different ferromagnetic properties with T_{c1} of about 30 K and T_{c2} of over 300 K, respectively. From the transport measurements of a single MnSi NW device, we found that MnSi NWs show itinerant helimagnetic properties with T_{c1} of about 30 K and conjecture that T_{c2} of over 300 K is from tetragonal $MnSi_{1.7}$ film formed on a Si substrate. The single MnSi NW device we fabricated here shows a very low electrical resistivity of 544 μΩcm and a large negative MR of −20% near T_c of about 30 K.

METHODS

Growth of MnSi NWs. Metal halide precursor is evaporated and transported to the higher temperature zone by a carrier gas, where decomposition of metal halide and reaction with the pre-heated silicon substrate occurs. Typically, MnSi NWs with a native oxide layer were synthesized on Si(100) substrates. The substrates were placed in the downstream zone in a conventional two-zone horizontal hot-wall furnace. Anhydrous $MnCl_2$ precur-

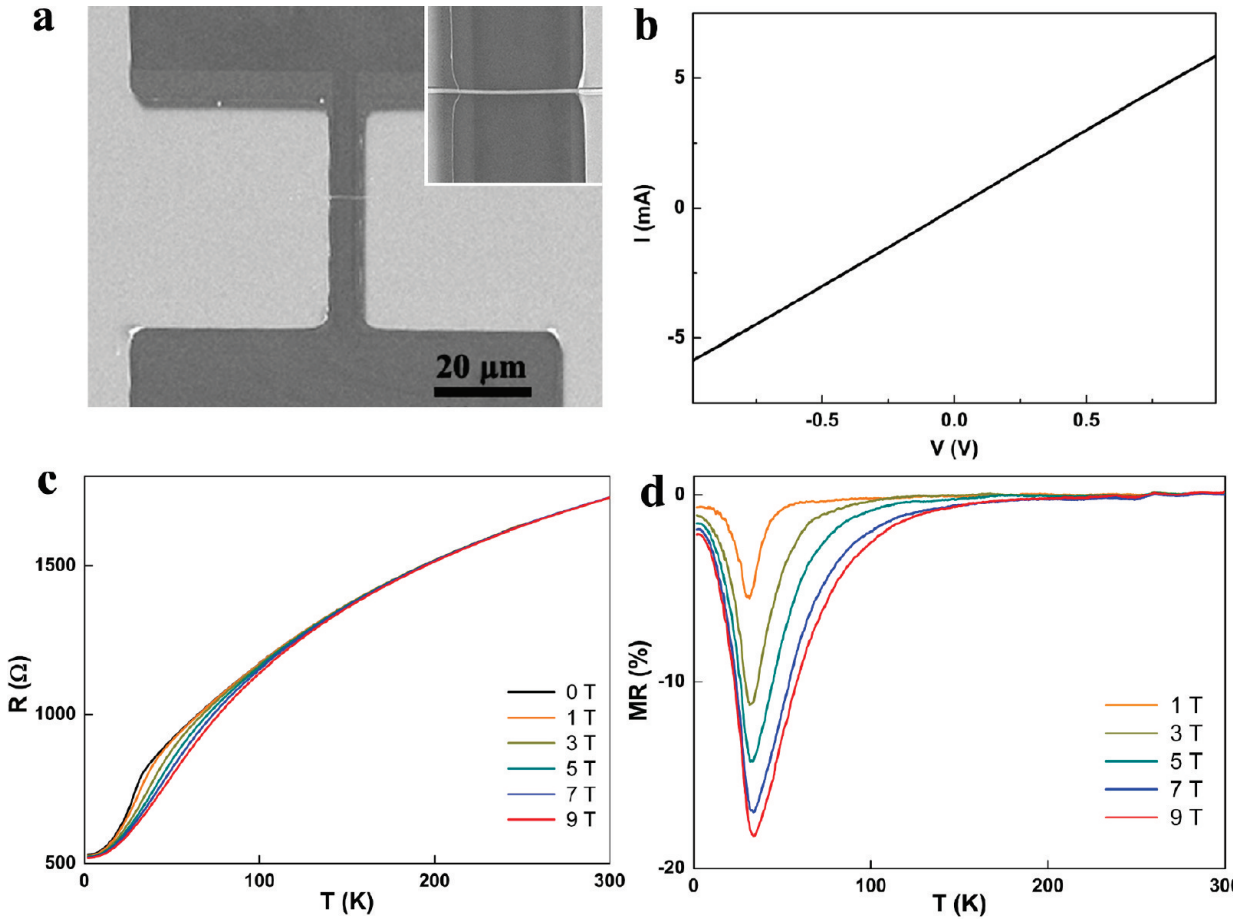

Figure 7. Electrical and magnetic properties of an individual MnSi NW. (a) SEM image of the MnSi NW device. Inset shows a magnified SEM image of the MnSi NW lying between the Au electrodes. (b) *I*−*V* curve recorded on the MnSi NW device by two-probe measurement. (c) Temperature-dependent resistance curves under various external magnetic fields. (d) Temperature-dependent MR (%) curves of a single MnSi NW under various external magnetic fields.

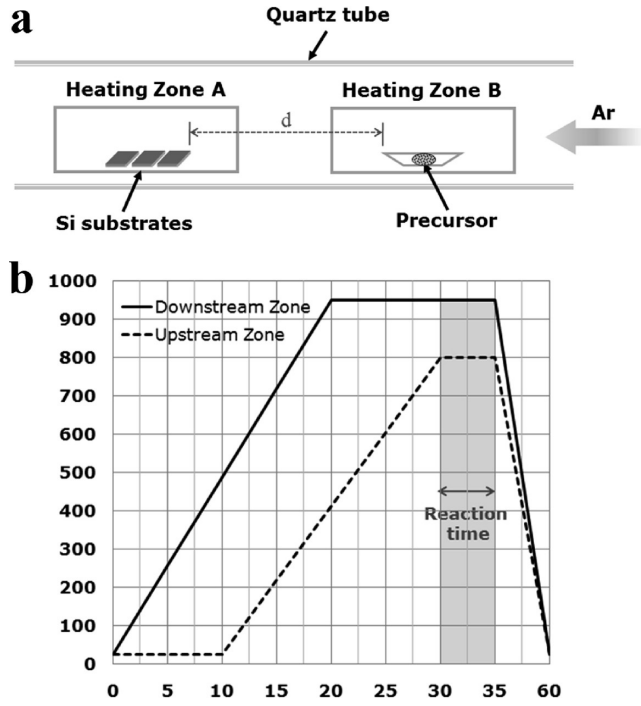

Figure 8. (a) Experimental setup and (b) reaction condition for synthesis of MnSi NWs.

sor (0.05 g, 99.999%, Sigma-Aldrich) was placed in an alumina boat in the upstream zone. The temperatures of the two zones were independently controlled. The system was purged with Ar gas for 30 min before each reaction for an inert atmosphere. The Ar flow rate of was about 200 sccm to synthesize the NWs. The substrates were placed at ~20 cm (*d* value in Figure 8a) from the precursor position in the downstream zone. The Ar gas transported precursor vapor produced at 800 °C to the downstream zone at 950 °C, where $MnCl_2$ decomposed and reacted with the Si substrate to form free-standing MnSi NWs. The reaction time was about 5 min (Figure 8b).

Device Fabrication of a Single MnSi NW. A thin oxide layer (SiO_2) of 10 nm and nitride layer (Si_3N_4) of 50 nm were thermally grown and deposited by low-pressure chemical vapor deposition (LPCVD), respectively, on a (100) Si wafer. Afterward, photoresist (AZ2035, AZ Electronic Materials) was patterned by photolithography (Figure 6a and Table S1 in Supporting Information). Subsequently, the nitride layer was partially etched by the wet etchant of 50% diluted HF solution for 50 s with a 12 nm/min etch rate. This partially recessed profile of the nitride will make the NWs fully wrapped by the subsequent metal electrodes. We reduced misalignment between the electrode and NW by the protruded nitride alignment marker after the aforementioned recess process. After removal of the photoresist (Figure 6g), the NW was positioned at the designed area by a nanomanipulator (Figure 6c). Nanomanipulator (SFS-H60XYZ, Sigma Koki), which can travel about 25 mm with a minimum increment of 1 nm, is a mechanical system to handle a nanometer-scale object in real-time using the attractive van der Waals force between the tip of the nanomanipulator and the object. The manipulator renders motions in *x*, *y*, and *z* directions, providing various manipulation freedoms such as moving and bending. Then, as shown in

Figure 6d,e, photoresist patterns were formed on the NWs again by use of the same lithography conditions in Table S1. Afterward, a thin gold of 150 nm was sputtered on the devices for 2.5 min with Ar flow rate of 25 sccm, pressure of 2.5 mTorr, and power of 250 W (Korea vacuum). Thereafter, the photoresist patterns were lifted off through dipping and sonication in an acetone solvent for 10 min and 10 s, respectively (Figure 6f). The fully wrapped MnSi NW devices were fabricated, as shown in Figure 6h.

Characterization. XRD patterns of the specimen were recorded on a Rigaku D/max-rc (12 kW) diffractometer operated at 40 kV and 80 mA with filtered 0.15405 nm Cu Kα radiation. FESEM images of MnSi NWs were taken on a Phillips XL30S. TEM and HR-TEM images and SAED patterns were taken on a JEOL JEM-2100F TEM operated at 200 kV.

Acknowledgment. This research was supported by KOSEF through NRL (2009-0083138), SRC (2010-0001484), and "Center for Nanostructured Material Technology" under "21st Century Frontier R&D Programs" (2009-K000468) of the MEST, Korea. SEM and TEM analysis were performed at the KBSI in Daejeon. The work of Y. Jo was supported by KBSI grant (T30513).

Supporting Information Available: Cross-sectional SEM images, additional HRTEM and TEM-EDS spectra, *M*(*H*) curve at 40 K, and detailed photoresist patterning conditions in device fabrication for the MnSi NWs. This material is available free of charge *via* the Internet at http://pubs.acs.org.

REFERENCES AND NOTES

1. Manyala, N.; DiTusa, J. F.; Aeppli, G.; Ramirez, A. P. Doping a Semiconductor To Create an Unconventional Metal. *Nature* **2008**, *454*, 976.
2. Cava, R. J.; Batlogg, B.; van Dover, R. B.; Murphy, D. W.; Sunshine, S.; Siegrist, T.; Remeika, J. P.; Rietman, E. A.; Zahurak, S.; Espinosa, G. P. Bulk Superconductivity at 91 K in Single-Phase Oxygen-Deficient Perovskite $Ba_2YCu_3O_{9-\delta}$. *Phys. Rev. Lett.* **1987**, *58*, 1676.
3. Manyala, N.; Sidis, Y.; DiTusa, J. F.; Aeppli, G.; Young, D. P.; Fisk, Z. Magnetoresistance from Quantum Interference Effects in Ferromagnets. *Nature* **2000**, *404*, 581.
4. Pfleiderer, C.; McMullan, G. J.; Julian, S. R.; Lonzarich, G. G. Magnetic Quantum Phase Transition in MnSi under Hydrostatic Pressure. *Phys. Rev. B* **1997**, *55*, 8330.
5. Pfleiderer, C.; Julian, S. R.; Lonzarich, G. G. Non-Fermi-Liquid Nature of the Normal State of Itinerant-Electron Ferromagnets. *Nature* **2001**, *414*, 427.
6. Pfleiderer, C.; Reznik, D.; Pintschovius, L.; Löhneysen, H. v.; Garst, M.; Rosch, A. Partial Order in the Non-Fermi-Liquid Phase of MnSi. *Nature* **2004**, *427*, 227.
7. Doiron-Leyraud, N.; Walker, I. R.; Taillefer, L.; Steiner, M. J.; Julian, S. R.; Lonzarich, G. G. Fermi-Liquid Breakdown in the Paramagnetic Phase of a Pure Metal. *Nature* **2003**, *425*, 595.
8. Pfleiderer, C.; Böni, P.; Keller, T.; Rössler, U. K.; Rosch, A. Non-Fermi Liquid Metal without Quantum Criticality. *Science* **2007**, *316*, 1871.
9. Arora, P.; Chattopadhyay, M. K.; Roy, S. B. Magnetocaloric Effect in MnSi. *Appl. Phys. Lett.* **2007**, *91*, 062508.
10. Gottlieb, U.; Sulpice, A.; Lambert-Andron, B.; Laborde, O. Magnetic Properties of Single Crystalline Mn_4Si_7. *J. Alloys Compd.* **2003**, *361*, 13.
11. Aoyama, I.; Kaibe, H.; Rauscher, L.; Kanda, T.; Mukoujima, M.; Sano, S.; Tsuji, T. Doping Effects on Thermoelectric Properties of Higher Manganese Silicides (HMSs, $MnSi_{1.74}$) and Characterization of Thermoelectric Generating Module Using p-Type (Al, Ge and Mo)-Doped HMSs and n-Type $Mg_2Si_{0.4}Sn_{0.6}$ Legs. *Jpn. J. Appl. Phys.* **2005**, *44*, 4275.
12. Aoyama, I.; Fedorov, M. I.; Zaitsev, V. K.; Solomkin, F. Y.; Eremin, I. S.; Samunin, A. Y.; Mukoujima, M.; Sano, S.; Tsuji, T. Effects of Ge Doping on Micromorphology of MnSi in $MnSi_{\sim 1.7}$ and on Their Thermoelectric Transport Properties. *Jpn. J. Appl. Phys.* **2005**, *44*, 8562.
13. Kamilov, T. S.; Chirva, V. P.; Kabilov, D. K. Photoelectric Properties of Higher Manganese Silicide (HMS)−Si<Mn>−M Structures. *Semicond. Sci. Technol.* **1999**, *14*, 1012.
14. Beach, G. S. D.; Nistor, C.; Knutson, C.; Tsoi, M.; Erskine, J. L. Dynamics of Field-Driven Domain-Wall Propagation in Ferromagnetic Nanowires. *Nat. Mater.* **2005**, *4*, 741.
15. Law, M.; Greene, L. E.; Johnson, J. C.; Saykally, R.; Yang, P. Nanowire Dye-Sensitized Solar Cells. *Nat. Mater.* **2005**, *4*, 455.
16. Hochbaum, A. I.; Chen, R.; Delgado, R. D.; Liang, W.; Garnett, E. C.; Najarian, M.; Majumdar, A.; Yang, P. Enhanced Thermoelectric Performance of Rough Silicon Nanowires. *Nature* **2008**, *451*, 163.
17. Boukai, A. I.; Bunimovich, Y.; Tahir-Kheli, J.; Yu, J.-K.; Goddard, W. A., III; Heath, J. R. Silicon Nanowires as Efficient Thermoelectric Materials. *Nature* **2008**, *451*, 168.
18. Seo, K.; Varadwaj, K. S. K.; Mohanty, P.; Lee, S.; Jo, Y.; Jung, M.-H.; Kim, J.; Kim, B. Magnetic Properties of Single-Crystalline CoSi Nanowires. *Nano Lett.* **2007**, *7*, 1240.
19. Higgins, J. M.; Schmitt, A. L.; Guzei, I. A.; Jin, S. Higher Manganese Silicide Nanowires of Nowotny Chimney Ladder Phase. *J. Am. Chem. Soc.* **2008**, *130*, 16086.
20. Ham, M.-H.; Lee, J.-W.; Moon, K.-J.; Choi, J.-H.; Myoung, J.-M. Single-Crystalline Ferromagnetic Mn_4Si_7 Nanowires. *J. Phys. Chem. C* **2009**, *113*, 8143.
21. Decker, C. A.; Solanki, R.; Freeouf, J. L.; Carruthers, J. R.; Evans, D. R. Directed Growth of Nickel Silicide Nanowires. *Appl. Phys. Lett.* **2004**, *84*, 1389.
22. Kim, C.-J.; Kang, K.; Woo, Y. S.; Ryu, K.-G.; Moon, H.; Kim, J.-M.; Zang, D.-S.; Jo, M.-H. Spontaneous Chemical Vapor Growth of NiSi Nanowires and Their Metallic Properties. *Adv. Mater.* **2007**, *19*, 3637.
23. Seo, K.; Varadwaj, K. S. K.; Cha, D.; In, J.; Kim, J.; Park, J.; Kim, B. Synthesis and Electrical Properties of Single Crystalline $CrSi_2$ Nanowires. *J. Phys. Chem. C* **2007**, *111*, 9072.
24. Yoon, H.; Seo, K.; Moon, H.; Varadwaj, K. S. K.; In, J.; Kim, B. Aluminum Foil Mediated Noncatalytic Growth of ZnO Nanowire Arrays on an Indium Tin Oxide Substrate. *J. Phys. Chem. C* **2008**, *112*, 9181.
25. Wu, H.; Hortamani, M.; Kratzer, P.; Scheffler, M. First-Principles Study of Ferromagnetism in Epitaxial Si−Mn Thin Films on Si(001). *Phys. Rev. Lett.* **2004**, *92*, 237202.
26. Ouyang, L.; Thrall, E. S.; Deshmukh, M. M.; Park, H. Vapor-Phase Synthesis and Characterization of ε-FeSi Nanowires. *Adv. Mater.* **2006**, *18*, 1437.
27. Varadwaj, K. S. K.; Seo, K.; In, J.; Mohanty, P.; Park, J.; Kim, B. Phase-Controlled Growth of Metastable Fe_5Si_3 Nanowires by a Vapor Transport Method. *J. Am. Chem. Soc.* **2007**, *129*, 8594.
28. Kang, K.; Kim, S.-K.; Kim, C.-J.; Jo, M.-H. The Role of NiO_x Overlayers on Spontaneous Growth of $NiSi_x$ Nanowires from Ni Seed Layers. *Nano Lett.* **2008**, *8*, 431.
29. Chueh, Y.-L.; Ko, M.-T.; Chou, L.-J.; Chen, L.-J.; Wu, C.-S.; Chen, C.-D. $TaSi_2$ Nanowires: A Potential Field Emitter and Interconnect. *Nano Lett.* **2006**, *6*, 1637.
30. Schmitt, A. L.; Bierman, M. J.; Schmeisser, D.; Himpsel, F. J.; Jin, S. Synthesis and Properties of Single-Crystal FeSi Nanowires. *Nano Lett.* **2006**, *6*, 1617.
31. Song, Y.; Schmitt, A. L.; Jin, S. Ultralong Single-Crystal Metallic Ni_2Si Nanowires with Low Resistivity. *Nano Lett.* **2007**, *7*, 965.
32. Song, Y.; Jin, S. Synthesis and Properties of Single-Crystal β_3-Ni_3Si Nanowires. *Appl. Phys. Lett.* **2007**, *90*, 173122.
33. Lin, H.-K.; Tzeng, Y.-F.; Wang, C.-H.; Tai, N.-H.; Lin, I.-N.; Lee, C.-Y.; Chiu, H.-T. Ti_5Si_3 Nanowire and Its Field Emission Property. *Chem. Mater.* **2008**, *20*, 2429.
34. Yu, L.; Ma, Y.; Zhu, J.; Feng, H.; Wu, Q.; Lu, Y.; Lin, W.; Sang, H.; Hu, Z. An *In-Situ* Chloride-Generated Route to Various One-Dimensional Nanostructures of Chromium-Based Compounds. *J. Phys. Chem. C* **2008**, *112*, 5865.
35. Schmitt, A. L.; Zhu, L.; Schmeiβer, D.; Himpsel, F. J.; Jin, S. Metallic Single-Crystal CoSi Nanowires *via* Chemical Vapor Deposition of Single-Source Precursor. *J. Phys. Chem. B* **2006**, *110*, 18142.
36. Seo, K.; Lee, S.; Yoon, H.; In, J.; Varadwaj, K. S. K.; Jo, Y.;

Jung, M.-H.; Kim, J.; Kim, B. Composition-Tuned Co_nSi Nanowires: Location-Selective Simultaneous Growth along Temperature Gradient. *ACS Nano* **2009**, *3*, 1145.
37. Xia, Y.; Yang, P.; Sun, Y.; Wu, Y.; Mayers, B.; Gates, B.; Yin, Y.; Kim, F.; Yan, H. One-Dimensional Nanostructures: Synthesis, Characterization, and Applications. *Adv. Mater.* **2003**, *15*, 353.
38. Pan, Z. W.; Dai, Z. R.; Wang, Z. L. Nanobelts of Semiconducting Oxides. *Science* **2001**, *291*, 1947.
39. Zhang, Y.; Wang, N.; Gao, S.; He, R.; Miao, S.; Liu, J.; Zhu, J.; Zhang, X. A Simple Method To Synthesize Nanowires. *Chem. Mater.* **2002**, *14*, 3564.
40. Dai, Z. R.; Pan, Z. W.; Wang, Z. L. Novel Nanostructures of Functional Oxides Synthesized by Thermal Evaporation. *Adv. Funct. Mater.* **2003**, *13*, 9.
41. Lee, G. H.; Huh, S. H.; Jeong, J. W.; Choi, B. J.; Kim, S. H.; Ri, H.-C. Anomalous Magnetic Properties of MnO Nanoclusters. *J. Am. Chem. Soc.* **2002**, *124*, 12094.
42. Seo, W. S.; Jo, H. H.; Lee, K.; Kim, B.; Oh, S. J.; Park, J. T. Size-Dependent Magnetic Properties of Colloidal Mn_3O_4 and MnO Nanoparticles. *Angew. Chem., Int. Ed.* **2004**, *43*, 1115.
43. Eizenberg, M.; Tu, K. N. Formation and Schottky Behavior of Manganese Silicide on n-Type Silicon. *J. Appl. Phys.* **1982**, *53*, 6885.